International Journal of Modern Physics C
Vol. 23, No. 6 (2012) 1250048 (16 pages)

DOI: 10.1142/S0129183112500489

STABILIZATION ANALYSIS OF A MULTIPLE LOOK-AHEAD MODEL WITH DRIVER REACTION DELAYS

JIANZHONG CHEN* and ZHONGKE SHI

College of Automation, Northwestern Polytechnical University
Xi'an, Shaanxi 710072, P. R. China
**jzhchen@nwpu.edu.cn*

YANMEI HU

College of Science, Chang'an University
Xi'an, Shaanxi 710064, P. R. China

Received 20 December 2011
Accepted 21 May 2012
Published 29 June 2012

A multiple look-ahead model is extended to take into account the reaction-time delay of drivers. The stability condition of this model is obtained by using the linear stability theory. Through nonlinear analysis, the Korteweg–de Vries (KdV) equation near the neutral stability line and the modified KdV (mKdV) equation near the critical point are derived. Both the analytical and simulation results demonstrate that the stabilization of traffic flow is weakened with increasing the reaction-time delay of drivers, and multiple look-ahead consideration could partially remedy this unfavorable effect.

Keywords: Multiple look-ahead model; driver reaction delays; traffic flow; stability analysis; density wave.

PACS Nos.: 02.60.Cb, 05.70.Fh, 05.70.Jk, 89.40.-a.

1. Introduction

Various traffic flow models have been developed to understand and analyze complex traffic flow phenomena in the past decades. Among them, the car-following models can describe the behavior of individual vehicles and drivers by differential equations. Newell and Whitham have proposed and analyzed a car-following model in the form of first-order differential-difference equation with the delay time.[1,2] The optimal velocity (OV) model[3] is one of well studied car-following models. By introducing the velocity difference term, a generalized force (GF) model and a full velocity difference (FVD) model have been developed.[4,5]

In recent years, the extension of the OV model and the FVD model to take into account many-neighbor interaction has received considerable attention.[6−19] Sawada has proposed a generalized OV function to describe the next-nearest-neighbor interaction.[6,7] Lenz *et al.* have presented an extended OV model by incorporating multi-vehicle interactions.[8] Wilson *et al.* have discussed two types of multiple look-ahead models.[9] In the model referred to Wilson *et al.* as model A, the optimal velocity of a driver is a weighted sum of multiple drivers' optimal velocity functions evaluated at their own headway.

In real traffic situations, drivers need time to sense velocity and position variations of the vehicles, make decisions and perform control actions. Hence, the reaction-time delay of drivers plays a crucial role in understanding traffic dynamics and constructing realistic models for traffic flow.

Chandler *et al.* have proposed the first car-following model including the time delay.[20] The original OV model has been extended to include an explicit delay time in Ref. 21. In this delay model, the headway and the own velocity are both evaluated at the delayed time. This means that drivers react to both their headway and their velocities via the delay time. Treiber *et al.* have taken a similar view, i.e., all input stimuli need to be evaluated at the delayed time when they extend the Intelligent Driver Model (IDM)[22] to human driver model (HDM).[23] Based on numerical simulations, Davis has investigated another time-delayed OV model in which only the argument of the headway contains delay due to driver reaction time.[24,25] Orosz *et al.* have presented the global bifurcation analysis of this delayed model.[26] The continuation results have been extended to large numbers of cars.[27]

The stability analysis of traffic models including driver reaction delays is important because introducing time delays may change the stability characteristics. For instance, a stable delay-free dynamics may become unstable. Therefore, it is necessary to perform a thorough stability analysis for time-delayed traffic flow models. Yu *et al.* have analyzed the time-delayed OV model[24] by the linear stability theory and nonlinear analysis method.[28] Zhu and Dai have proposed an extended car-following model including the driver's physical delay and derived the Korteweg−de Vries (KdV) equation and modified KdV (mKdV) equation.[29] Ge *et al.* have derived the time-dependent Ginzburg−Landau (TDGL) equation from this model.[30] In the time-delayed models,[28−30] drivers are assumed to only react to the actions of the preceding vehicle. With the development and application of the intelligent transportation systems (ITS), drivers can obtain information of multiple leading vehicles in traffic. However, the multiple look-ahead models with driver reaction delays and the relevant stability analysis have not been studied.

In this paper, we incorporate the reaction-time delay of drivers into a multiple look-ahead model. The stability analysis and density waves of this model are presented. The linear stability analysis is given to show the stabilization effect of including driver reaction delays. Moreover, we apply the nonlinear analysis to derive the KdV equation near the neutral stability line and the mKdV equation near the critical point to describe traffic jams. Finally, numerical simulations are carried out.

2. Model

The OV model[3] can be written in following differential equation:

$$\frac{\mathrm{d}v_n(t)}{\mathrm{d}t} = a[V(\triangle x_n) - v_n(t)], \tag{1}$$

where $x_n(t)$ is the position of the nth car at time t, $\triangle x_n = x_{n+1} - x_n$ represents the headway of the nth car, a denotes the sensitivity of a driver and V is the OV function.

The model (1) can describe a variety of real traffic phenomena, but has some disadvantages such as too high acceleration and unrealistic deceleration. To remedy the deficiencies of the OV model, Wilson *et al.* have proposed a multiple look-ahead model[9] given by

$$\frac{\mathrm{d}v_n(t)}{\mathrm{d}t} = a\left[\sum_{l=1}^{m} \beta_l V(\triangle x_{n+l-1}(t)) - v_n(t)\right], \tag{2}$$

where β_l is a weight of the OV function $V(\triangle x_{n+l-1})$. Equation (2) shows that drivers do not only react to the actions of the leading vehicle but also take into consideration up to m vehicles in front. When we incorporate the reaction-time delay of drivers τ_d into the model (2), we obtain the following delayed model:

$$\frac{\mathrm{d}v_n(t)}{\mathrm{d}t} = a\left[\sum_{l=1}^{m} \beta_l V(\triangle x_{n+l-1}(t-\tau_d)) - v_n(t)\right]. \tag{3}$$

Here, it is assumed that drivers can react to their own velocity immediately and only the headway $\triangle x_{n+l-1}$ is evaluated at the delayed time. It is important to note that τ_d is different from the characteristic relaxation time $\tau = 1/a$ which represents the time for adjustment of the vehicles' velocities.

Based on an analysis of the properties of weight in Ref. 31, the weight β_l is chosen as

$$\sum_{l=1}^{m} \beta_l = 1, \quad \beta_l = \begin{cases} (r-1)/r^l & \text{for } l \neq m, \\ 1/r^{l-1} & \text{for } l = m, \end{cases} \tag{4}$$

where the constant r can be taken as $r = 2, 3, \ldots$. Note that as the distance between the considered car and the preceding cars increases the effect of preceding cars on the car motion reduces gradually. In our simulations, r is set to 6.

The OV function $V(\triangle x_n(t))$ is chosen similar to that introduced in Ref. 3

$$V(\triangle x_n(t)) = \frac{v_{\max}}{2}[\tanh(\triangle x_n(t) - h_c) + \tanh(h_c)], \tag{5}$$

where $v_{\max}$ is the maximum velocity and h_c is the safety distance. Note that this OV function has a turning point at $\triangle x_n = h_c$, i.e., $V''(h_c) = 0$, which is important for us to obtain the kink−antikink density wave solution describing the traffic jam in the unstable region.

3. Linear Stability Analysis

In this section, we carry out the linear stability analysis for Eq. (3). The steady state solution for Eq. (3) is given by

$$x_n^{(0)}(t) = hn + V(h)t, \quad h = L/N, \tag{6}$$

where N is total number of vehicles, L is the length of the road and h is the average headway. Suppose that $y_n(t)$ is a small deviation from the steady state solution $x_n^{(0)}(t) : x_n(t) = x_n^{(0)}(t) + y_n(t)$. By substituting it into Eq. (3) and linearizing the resulting equation, one can obtain

$$\frac{\mathrm{d}^2 y_n(t)}{\mathrm{d}t^2} = a\left[\sum_{l=1}^{m} \beta_l V'(h)(\triangle y_{n+l-1}(t-\tau_d)) - \frac{\mathrm{d}y_n(t)}{\mathrm{d}t}\right], \tag{7}$$

where $\triangle y_n = y_{n+1} - y_n$ and $V'(h) = \mathrm{d}V(\triangle x_n)/\mathrm{d}\triangle x_n|_{\triangle x_n = h}$.

By expanding $y_n(t) = Y\exp(\mathrm{i}kn + zt)$, one obtains the following equation of z

$$z^2 + az - aV'(h)\mathrm{e}^{-z\tau_d}\sum_{l=1}^{m}\beta_l(\mathrm{e}^{ikl} - \mathrm{e}^{ik(l-1)}) = 0. \tag{8}$$

Expanding $z = z_1(\mathrm{i}k) + z_2(\mathrm{i}k)^2 + \cdots$ and inserting it into Eq. (8), we obtain the first- and second-order terms of coefficients in the expression of z respectively, which are given by

$$z_1 = V'(h), \quad z_2 = -\frac{z_1^2}{a} + \frac{V'(h)}{2}\sum_{l=1}^{m}\beta_l(2l-1) - z_1^2\tau_d. \tag{9}$$

The uniformly steady-state flow is unstable for long-wavelength modes if $z_2 < 0$ and stable if $z_2 > 0$. Consequently, the neutral stability condition is given by

$$a = \frac{2V'(h)}{\sum_{l=1}^{m}\beta_l(2l-1) - 2V'(h)\tau_d}. \tag{10}$$

For small disturbances of long wavelengths, the uniform traffic flow is unstable if the following condition holds

$$a < \frac{2V'(h)}{\sum_{l=1}^{m}\beta_l(2l-1) - 2V'(h)\tau_d}. \tag{11}$$

Figures 1 and 2 show the neutral stability curves (solid lines) in the space $(\Delta x, a)$ for different parameters m and τ_d, respectively. The apex of each curve indicates the critical point (h_c, a_c). From Figs. 1 and 2, it can be seen that the critical points and the neutral stability curves will be lowered with the increase of m or with the decrease of τ_d. This means that by considering more vehicles ahead or smaller drivers' reaction delay the traffic flow will be more stable. The effect on the stability of traffic flow by considering multiple look-ahead and driver reaction

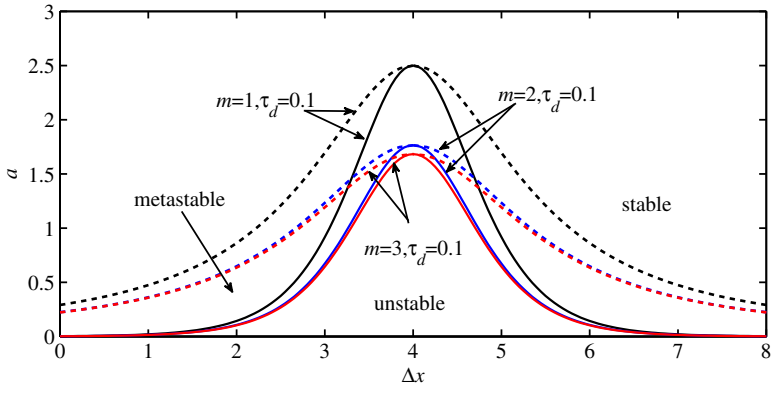

Fig. 1. (Color online) Phase diagram in the headway-sensitivity space for different values of m with $\tau_d = 0.1$. ($v_{\max} = 2.0$, $h_c = 4.0$).

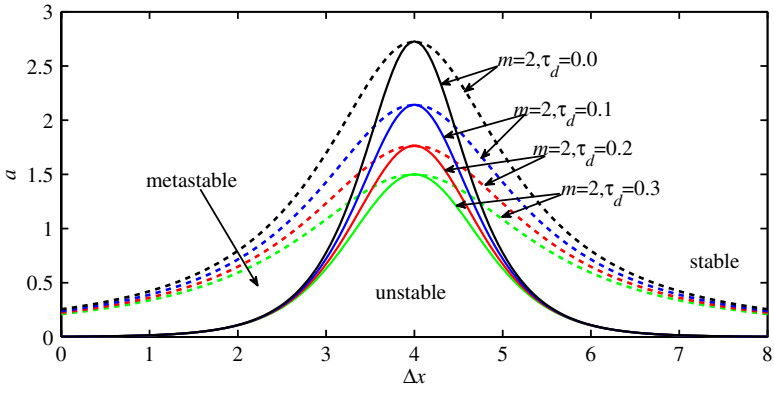

Fig. 2. (Color online) Phase diagram in the headway-sensitivity space for $m = 2$ with different values of τ_d. ($v_{\max} = 2.0$, $h_c = 4.0$).

delays can be further illustrated in Fig. 3. Neutral stability lines (solid lines) for the cases of $m = 1$ and $m = 3$ with different values of τ_d are plotted. It can be found that the unstable regions for $m = 3$ are slightly smaller than those for $m = 1$ when the difference of time delay of both cases is 0.2. This means that the unfavorable effect due to driver reaction delays could be partially remedied by multiple look-ahead consideration.

4. Nonlinear Stability Analysis

To investigate the effects of the reaction-time delay τ_d on the stability of traffic flow more fully, we next perform a nonlinear analysis to study the slowly varying behavior at long wavelengths near the neutral stability line and the critical point. For

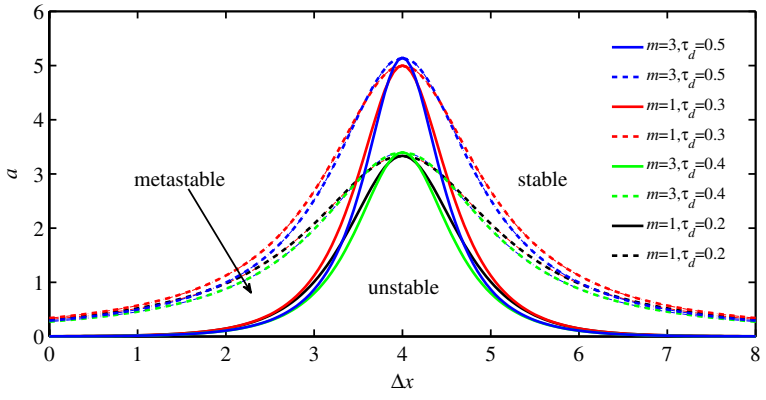

Fig. 3. (Color online) Phase diagram in the headway-sensitivity space for $m = 1, 3$ with different values of τ_d. ($v_{\max} = 2.0$, $h_c = 4.0$).

convenience, Eq. (3) can be rewritten in the form:

$$\frac{\mathrm{d}\Delta v_n(t)}{\mathrm{d}t} = a\left[\sum_{l=1}^{m}\beta_l V(\triangle x_{n+l}(t-\tau_d)) - \sum_{l=1}^{m}\beta_l V(\triangle x_{n+l-1}(t-\tau_d)) - \Delta v_n(t)\right]. \quad (12)$$

4.1. *KdV equation*

We will derive the KdV equation near the neutral curve. Introducing the slow scales for space variable n and time variable t, slow variables X and T are defined as follows[31–34]:

$$X = \varepsilon(n + bt), \quad T = \varepsilon^3 t, \quad 0 < \varepsilon \ll 1, \quad (13)$$

where b is a constant to be determined. The headway is set

$$\triangle x_n(t) = h + \varepsilon^2 R(X, T). \quad (14)$$

Substituting Eqs. (13) and (14) into Eq. (12) and making the Taylor expansions to the sixth-order of ε lead to

$$\begin{aligned}
&\varepsilon^3(b - V')\partial_X R + \varepsilon^4\left[\frac{b^2}{a} - \frac{V'}{2}\sum_{l=1}^{m}\beta_l(2(l - b\tau_d) - 1)\right]\partial_X^2 R \\
&\quad + \varepsilon^5\left\{\partial_T R - \left[\frac{V'}{6}\sum_{l=1}^{m}\beta_l(3(l - b\tau_d)^2 - 3(l - b\tau_d) + 1)\right]\partial_X^3 R - \frac{V''}{2}\partial_X R^2\right\} \\
&\quad + \varepsilon^6\left\{\left(\frac{2b}{a} + V'\tau_d\right)\partial_X\partial_T R\right.
\end{aligned}$$

$$- \left[\frac{V'}{24}\sum_{l=1}^{m}\beta_l(4(l-b\tau_d)^3 - 6(l-b\tau_d)^2 + 4(l-b\tau_d) - 1)\right]\partial_X^4 R$$
$$- \frac{V''}{4}\sum_{l=1}^{m}\beta_l(2(l-b\tau_d) - 1)\partial_X^2 R^2\Bigg\} = 0, \tag{15}$$

where $V' = V'(h) = \mathrm{d}V(\triangle x_n)/\mathrm{d}\triangle x_n|_{\triangle x_n = h}$ and $V'' = V''(h) = \mathrm{d}^2V(\triangle x_n)/\mathrm{d}\triangle x_n^2|_{\triangle x_n = h}$. Near the neutral stability line $a_s = 2V'(h)/[\sum_{l=1}^{m}\beta_l(2l-1) - 2V'(h)\tau_d]$, $a_s/a = 1 - \epsilon^2$. By setting $b = V'$ and eliminating the third- and fourth-order terms of ε from Eq. (15), we obtain

$$\varepsilon^5(\partial_T R - f_1\partial_X^3 R - f_2 R\partial_X R) + \varepsilon^6(-f_3\partial_X^2 R + f_4\partial_X^4 R + f_5\partial_X^2 R^2) = 0, \tag{16}$$

where

$$f_1 = \frac{V'}{6}\sum_{l=1}^{m}\beta_l(3(l-V'\tau_d)^2 - 3(l-V'\tau_d) + 1), \quad f_2 = V'',$$
$$f_3 = \frac{V'}{2}\sum_{l=1}^{m}\beta_l(2(l-V'\tau_d) - 1),$$
$$f_4 = \left(\frac{2V'}{a_s} + V'\tau_d\right)\left[\frac{V'}{6}\sum_{l=1}^{m}\beta_l(3(l-V'\tau_d)^2 - 3(l-V'\tau_d) + 1)\right]$$
$$+ \left[-\frac{V'}{24}\sum_{l=1}^{m}\beta_l(4(l-V'\tau_d)^3 - 6(l-V'\tau_d)^2 + 4(l-V'\tau_d) - 1)\right],$$
$$f_5 = \left(\frac{2V'}{a_s} + V'\tau_d\right)\frac{V''}{2} - \frac{V''}{4}\sum_{l=1}^{m}\beta_l(2(l-V'\tau_d) - 1).$$

To derive the standard KdV equation with higher-order correction, we make the following transformation for Eq. (16)

$$T = \sqrt{f_1}T', \quad X = -\sqrt{f_1}X', \quad R = \frac{1}{f_2}R', \tag{17}$$

so that Eq. (16) can be rewritten as

$$\partial_{T'}R' + \partial_{X'}^3 R' + R'\partial_{X'}R' + \frac{\varepsilon}{\sqrt{f_1}}\left[-f_3\partial_{X'}^2 R' + \frac{f_4}{f_1}\partial_{X'}^4 R' + \frac{f_5}{f_2}\partial_{X'}^2 R'^2\right] = 0. \tag{18}$$

Equation (18) is just the KdV equation after ignoring the $O(\varepsilon)$ term. The soliton solution of the KdV equation can be expressed as:

$$R_0'(X', T') = A\,\mathrm{sech}^2\left[\sqrt{\frac{A}{12}}\left(X' - \frac{A}{3}T'\right)\right], \tag{19}$$

where A is the amplitude of soliton solution that will be determined.

To take into account the $O(\varepsilon)$ correction, we assume that

$$R'(X',T') = R'_0(X',T') + \varepsilon R'_1(X',T'). \tag{20}$$

The following solvability condition should be satisfied to determine the amplitude A,

$$(R'_0, M[R'_0]) \equiv \int_{-\infty}^{+\infty} \mathrm{d}X' R'_0 M[R'_0] = 0, \tag{21}$$

where $M[R'_0]$ is the $O(\varepsilon)$ term of Eq. (18). Integration of (21) yields

$$A = \frac{21 f_1 f_2 f_3}{24 f_1 f_5 - 5 f_2 f_4}, \tag{22}$$

so the soliton solution of the headway is given by

$$\triangle x_n(t) = h + \frac{A}{f_2}\left(1 - \frac{a_s}{a}\right)\mathrm{sech}^2\left\{\sqrt{\frac{A}{12 f_1}\left(1 - \frac{a_s}{a}\right)} \times \left[n + V't + \frac{A}{3}\left(1 - \frac{a_s}{a}\right)t\right]\right\}. \tag{23}$$

4.2. *mKdV equation*

To derive the mKdV equation near the critical point, we still use the perturbation method as in the previous subsection. The slow variables X and T are defined in Eq. (13). The headway is set

$$\triangle x_n(t) = h_c + \varepsilon R(X,T). \tag{24}$$

Substituting Eqs. (13) and (24) into Eq. (12) and making the Taylor expansion to the fifth-order of ε, one can obtain

$$\begin{aligned}
&\varepsilon^2(b - V')\partial_X R + \varepsilon^3\left[\frac{b^2}{a} - \frac{V'}{2}\sum_{l=1}^{m}\beta_l(2(l - b\tau_d) - 1)\right]\partial_X^2 R \\
&\quad + \varepsilon^4\left\{\partial_T R - \left[\frac{V'}{6}\sum_{l=1}^{m}\beta_l(3(l - b\tau_d)^2 - 3(l - b\tau_d) + 1)\right]\partial_X^3 R - \frac{V'''}{6}\partial_X R^3\right\} \\
&\quad + \varepsilon^5\left\{\left(\frac{2b}{a} + V'\tau_d\right)\partial_X\partial_T R\right. \\
&\quad + \left[-\frac{V'}{24}\sum_{l=1}^{m}\beta_l(4(l - b\tau_d)^3 - 6(l - b\tau_d)^2 + 4(l - b\tau_d) - 1)\right]\partial_X^4 R \\
&\quad \left. - \frac{V'''}{12}\sum_{l=1}^{m}\beta_l(2(l - b\tau_d) - 1)\partial_X^2 R^3\right\} = 0,
\end{aligned} \tag{25}$$

where $V' = V'(h_c) = \mathrm{d}V(\triangle x_n)/\mathrm{d}\triangle x_n|_{\triangle x_n = h_c}$ and $V''' = V'''(h_c) = \mathrm{d}^3 V(\triangle x_n)/\mathrm{d}\triangle x_n^3|_{\triangle x_n = h_c}$. Near the critical point (h_c, a_c), $a_c/a = 1 + \epsilon^2$. By the choice of $b = V'$, the second- and third-order terms of ε are eliminated from Eq. (25). Then Eq. (25) can be rewritten in the form:

$$\varepsilon^4[\partial_T R - g_1 \partial_X^3 R + g_2 \partial_X R^3] + \varepsilon^5[g_3 \partial_X^2 R + g_4 \partial_X^4 R + g_5 \partial_X^2 R^3] = 0, \tag{26}$$

where

$$g_1 = \frac{V'}{6}\sum_{l=1}^{m} \beta_l (3(l - V'\tau_d)^2 - 3(l - V'\tau_d) + 1), \quad g_2 = -\frac{V'''}{6},$$

$$g_3 = \frac{V'}{2}\sum_{l=1}^{m} \beta_l (2(l - V'\tau_d) - 1),$$

$$g_4 = \left(\frac{2V'}{a_c} + V'\tau_d\right)\left[\frac{V'}{6}\sum_{l=1}^{m} \beta_l (3(l - V'\tau_d)^2 - 3(l - V'\tau_d) + 1)\right]$$
$$+ \left[-\frac{V'}{24}\sum_{l=1}^{m} \beta_l (4(l - V'\tau_d)^3 - 6(l - V'\tau_d)^2 + 4(l - V'\tau_d) - 1)\right],$$

$$g_5 = -\frac{V'''}{12}\left[\sum_{l=1}^{m} \beta_l (2(l - V'\tau_d) - 1) - \frac{4V'}{a_c} - 2V'\tau_d\right].$$

To derive the standard mKdV equation with higher-order correction, we use the following transformation formula

$$T = \frac{1}{g_1} T', \quad R = \sqrt{\frac{g_1}{g_2}} R'. \tag{27}$$

Substituting transformation (27) into Eq. (26), one can obtain the mKdV equation with an $O(\varepsilon)$ correction term

$$\partial_{T'} R' - \partial_X^3 R' + \partial_X R'^3 + \varepsilon \sqrt{\frac{1}{g_1}}\left[g_3 \partial_X^2 R' + g_4 \partial_X^4 R' + \frac{g_1 g_5}{g_2}\partial_X^2 R'^3\right] = 0. \tag{28}$$

After ignoring the $O(\varepsilon)$ term, Eq. (28) is just the mKdV equation. The kink−antikink solution of (28) can be expressed by

$$R_0'(X, T') = \sqrt{B}\tanh\left[\sqrt{\frac{B}{2}}(X - BT')\right], \tag{29}$$

where B is the propagation velocity. Using the similar manner to determine the amplitude A for KdV equation in the previous subsection, the velocity B can be computed as:

$$B = \frac{5g_2 g_3}{2g_2 g_4 - 3g_1 g_5}. \tag{30}$$

Thus, the solution of the mKdV equation is given by

$$R(X,T) = \sqrt{\frac{g_1 B}{g_2}} \tanh\left[\sqrt{\frac{B}{2}}\,(X - Bg_1 T)\right]. \tag{31}$$

By rewriting each variable to the original one, the general kink−antikink solution of the headway can be given by

$$\triangle x_n(t) = h_c + \sqrt{\frac{g_1 B}{g_2}\Big(\frac{a_c}{a} - 1\Big)} \tanh\left\{\sqrt{\frac{B}{2}\Big(\frac{a_c}{a} - 1\Big)} \times \Big[n + V't - Bg_1\Big(\frac{a_c}{a} - 1\Big)t\Big]\right\}. \tag{32}$$

Then the amplitude C of the solution is given by

$$C = \sqrt{\frac{g_1 B}{g_2}\Big(\frac{a_c}{a} - 1\Big)}. \tag{33}$$

The kink wave solution represents the coexisting phase, which includes the freely moving phase with low density and the jammed (or congested) phase with high density. The headways corresponding to the freely moving phase and the jammed phase can be computed by $\triangle x = h_c + C$ and $\triangle x = h_c - C$, respectively. Thus, we obtain the coexisting curve in the $(\Delta x, a)$ plane. The coexisting curve is depicted by dotted line in Figs. 1−3. From Figs. 1−3, it is found that the space is divided into three regions by each pair of solid line and dotted line. Above the coexisting curve and below the neutral stability curve are the stable region and the unstable region, respectively. The metastable region lies between the neutral stability curve and the coexisting curve.

From above analysis, the KdV and mKdV equations are derived. They depict the density waves appearing in the metastable and unstable regions, respectively.

5. Simulation

In this section, we use numerical experiments to investigate the effects of the drivers' reaction delays on the stability of traffic flow. The initial conditions are chosen as follows: $\triangle x_n(0) = h$, $\triangle x_n(1) = h$ for $j \neq 50, 51$, $\triangle x_n(1) = h - 0.5$ for $j = 50$ and $\triangle x_n(1) = h + 0.5$ for $j = 51$, where $h = 3.6$ is initial uniform headway. The total number of vehicles N is set as 100, the safety distance is $h_c = 4.0$ and the maximum velocity $v_{\max}$ is taken as 2.0. The periodic boundary conditions are adopted.

We first fix $\tau_d = 0.1$ to explore the effect of considering various number of vehicles in front. In Fig. 4, the patterns (a), (b), (c) and (d) illustrate the space-time evolution of the headway for $m = 1, 2, 3$ and 5, where $a = 1.39$. In patterns (a)−(d), the traffic flow is unstable since the instability condition (11) is satisfied for given parameters. Therefore, the kink−antikink density waves appear as traffic jams.

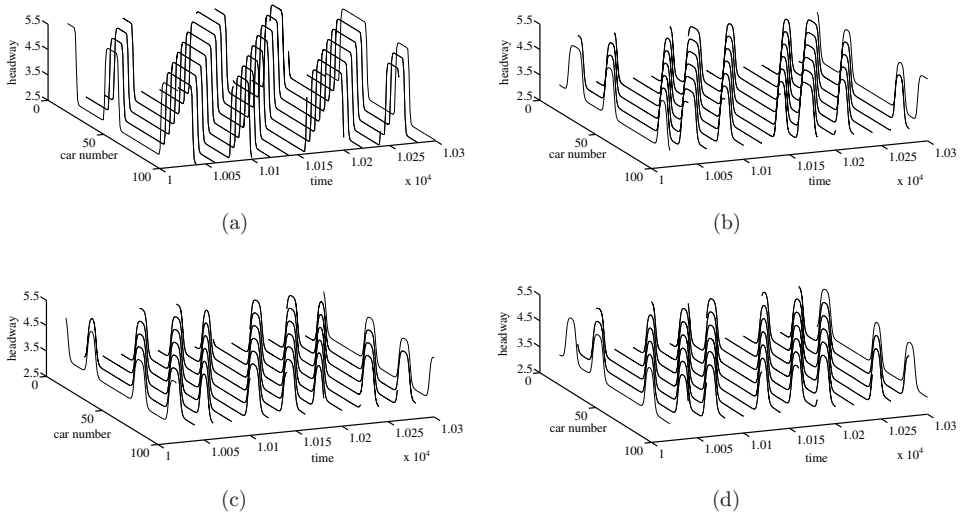

Fig. 4. Space-time evolution of the headway after $t = 10\,000$. The patterns (a), (b), (c) and (d) correspond to $m = 1, 2, 3$ and 5, respectively. ($a = 1.39, \tau_d = 0.1$).

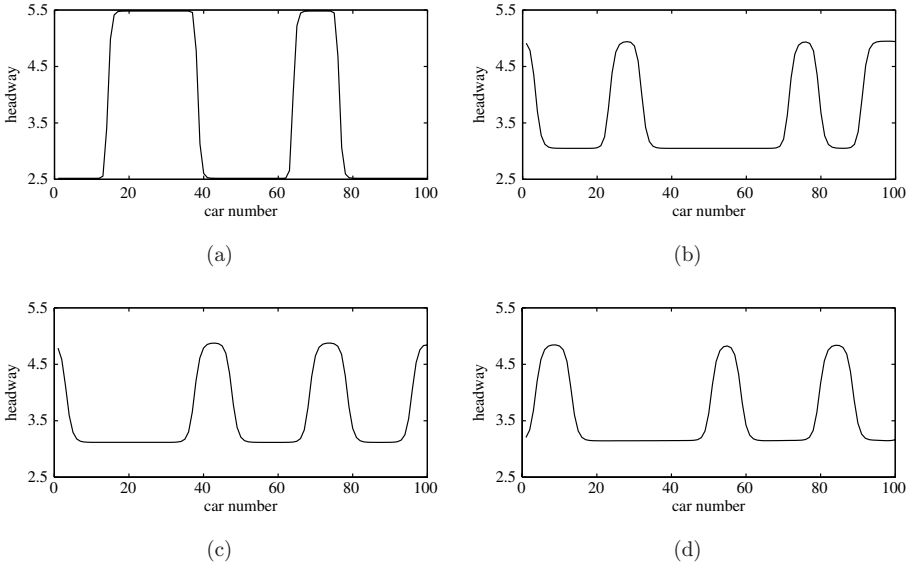

Fig. 5. Headway profiles of the density waves at $t = 10\,300$. The patterns (a), (b), (c) and (d) correspond to $m = 1, 2, 3$ and 5, respectively. ($a = 1.39, \tau_d = 0.1$).

The headway profiles at $t = 10\,300$ corresponding to Fig. 4 are shown in Fig. 5. From Fig. 5, we can see that the amplitude of the density wave decreases with increasing the number of the vehicles in front. Moreover, the impact of the vehicles ahead is almost invariant after $m = 3$. These results are similar to those

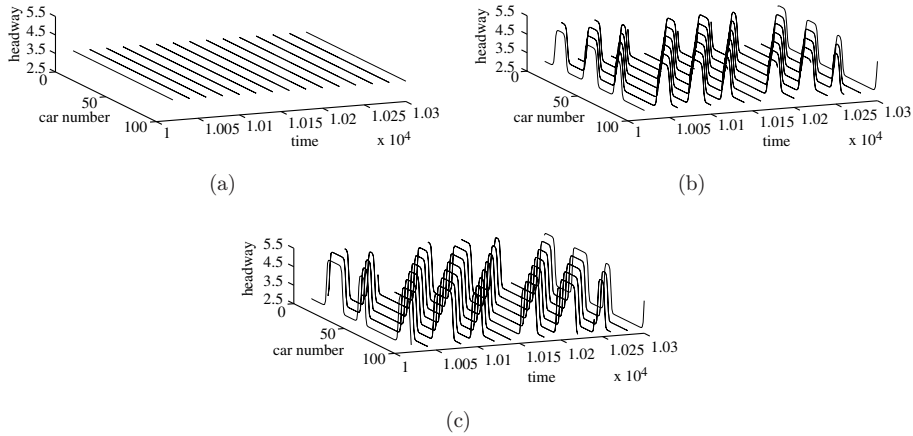

Fig. 6. Space-time evolution of the headway after $t = 10\,000$. The patterns (a), (b) and (c) correspond to $\tau_d = 0.3, 0.4$ and 0.5, respectively. $(a = 2.26, m = 3)$.

discussed in Refs. 18 and 19, in which the reaction-time delay of drivers is not considered.

Next, we choose $m = 3$ to study the influence of taking into account different reaction time. The patterns (a)−(c) in Fig. 6 exhibit the space-time evolution of the headway for $\tau_d = 0.3, 0.4$ and 0.5, where $a = 2.26$. When $\tau_d = 0.3$, the traffic flow is stable. In pattern (a) the density waves disappear and the traffic flow is uniform over the whole space. While in patterns (b) and (c), the traffic flow is unstable since the instability condition (11) is satisfied for $\tau_d = 0.4$ and 0.5. The kink−antikink density waves appear as traffic jams and the density waves propagate backward.

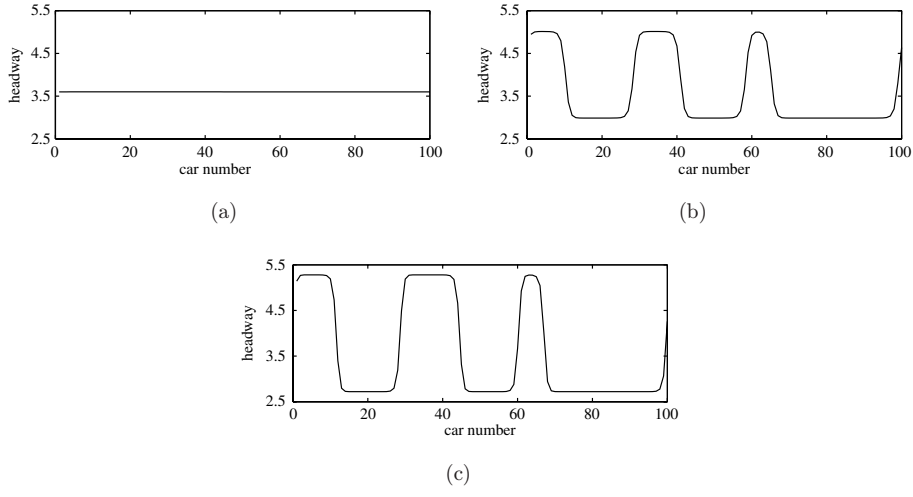

Fig. 7. Headway profiles of the density waves at $t = 10\,300$. The patterns (a), (b) and (c) correspond to $\tau_d = 0.3, 0.4$ and 0.5, respectively. $(a = 2.26, m = 3)$.

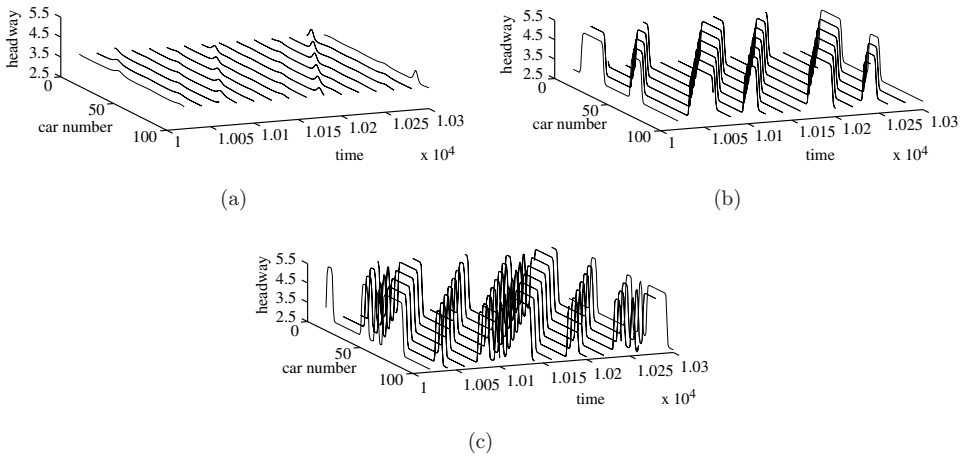

Fig. 8. Space-time evolution of the headway after $t = 10\,000$. The patterns (a), (b) and (c) correspond to $\tau_d = 0.1, 0.2$ and 0.3, respectively. $(a = 2.26, m = 1)$.

The headway profiles at $t = 10\,300$ corresponding to Fig. 6 are shown in Fig. 7. From Fig. 7, it can be seen that the amplitude of the density wave increases as the drivers' reaction delay increases.

For comparison, we also present the results for the case of $m = 1$ with the same sensitivity. Figure 8 shows the space-time evolution of the headway for $\tau_d = 0.1, 0.2$ and 0.3. When small disturbances are added to the uniform traffic flow, they are gradually magnified and the uniform flow evolves into an inhomogeneous one. In pattern (a) the soliton density waves appear as traffic jam. This is because the initial condition lies in the metastable region and near the neutral stability line. In patterns (b) and (c), the traffic flow is unstable because the instability condition (11) is satisfied for $\tau_d = 0.2$ and 0.3. The kink−antikink density waves appear as traffic jams.

The headway profiles at $t = 10\,300$ corresponding to Fig. 8 are shown in Fig. 9. Comparing the pattern (a) in Fig. 9 with the pattern (a) in Fig. 7, we can see that multiple look-ahead consideration could suppress the traffic jam. Comparing the patterns (b) and (c) in Fig. 9 with the patterns (b) and (c) in Fig. 7, we can see that the amplitude of the kink−antikink density wave for the case of $m = 3$ is lower than that for the case of $m = 1$ when the difference of time delay of both cases is 0.2. The results indicate multiple look-ahead consideration could partially remedy the stabilization effect caused by driver reaction delays.

Finally, we choose $m = 2$ and $a = 1.28$ to compare the theoretical and numerical results of the amplitude of the kink−antikink wave. The amplitude against τ_d is shown in Fig. 10. The solid line indicates the theoretical result calculated by Eq. (33). From Fig. 10, it can be found that the theoretical results of amplitude are smaller than the numerical ones. The reason is as below. To obtain the kink−antikink waves, we choose a small a to ensure the traffic flow is in the unstable region, which causes

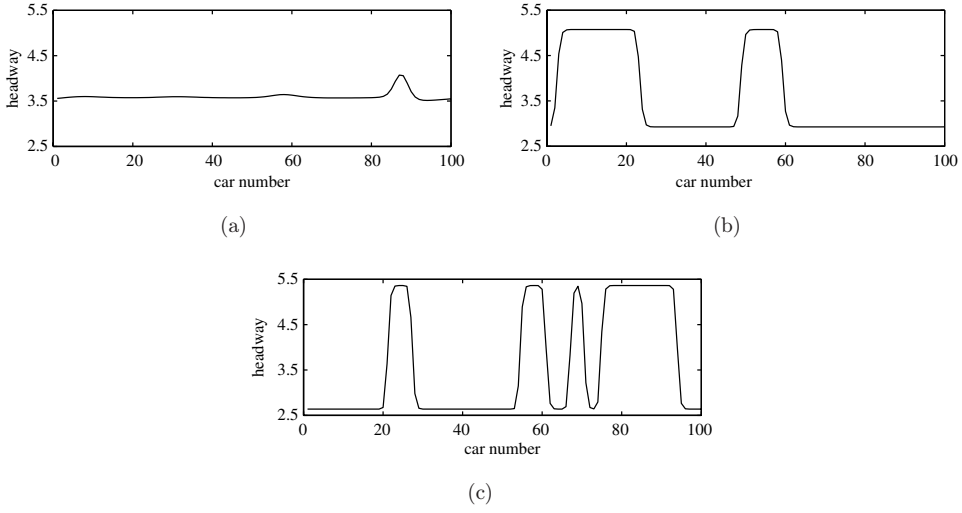

Fig. 9. Headway profiles of the density waves at $t = 10\,300$. The patterns (a), (b) and (c) correspond to $\tau_d = 0.1, 0.2$ and 0.3, respectively. $(a = 2.26, m = 1)$.

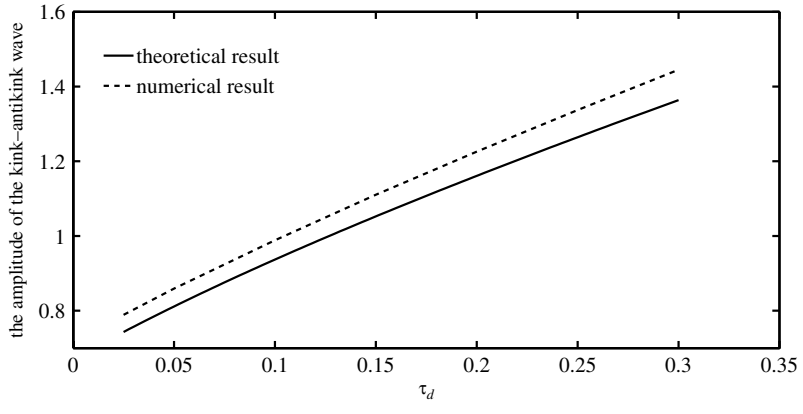

Fig. 10. The amplitude of the kink−antikink wave against τ_d for $m = 2$ and $a = 1.28$.

$\varepsilon = \sqrt{\frac{a_c}{a} - 1}$ is relatively big. Then the theoretical result is smaller than its actual value since we ignore the $O(\varepsilon)$ term in Eq. (18). Moreover, the value of ε increases with the increase of τ_d. Accordingly, the difference between the theoretical and numerical result also increases.

6. Conclusions

The reaction-time delay of drivers is a parameter that plays an important role in traffic flow models. We have incorporated the drivers' reaction delay into a multiple

look-ahead model in this paper. We have analyzed this model by using linear stability and nonlinear methods. The neutral stability line and the critical point are obtained. Moreover, the KdV equation near the neutral stability line and the mKdV equation near the critical point are derived by the use of the reductive perturbation method. The analytical and numerical results show that the reaction-time delay of drivers can weaken the stability of traffic flow and this unfavorable effect could be partially remedied by multiple look-ahead consideration.

Acknowledgments

This work was supported by the National Natural Science Foundation of China (Grant No. 11102165), NPU Foundation for Fundamental Research (Grant No. NPU-FFR-JC201254) and the Special Fund for Basic Scientific Research of Central Colleges, Chang'an University (Grant No. CHD2011JC039). The authors would like to thank the anonymous referees for their valuable suggestions on improving the paper.

References

1. G. F. Newell, *Oper. Res. Soc.* **9**, 209 (1961).
2. G. B. Whitham, *Proc. Roy. Soc. Lond. Ser. A* **428**, 49 (1990).
3. M. Bando, K. Hasebe, A. Nakayama, A. Shibata and Y. Sugiyama, *Phys. Rev. E* **51**, 1035 (1995).
4. D. Helbing and B. Tilch, *Phys. Rev. E* **58**, 133 (1998).
5. R. Jiang, Q. S. Wu and Z. J. Zhu, *Phys. Rev. E* **64**, 017101 (2001).
6. S. Sawada, *Int. J. Mod. Phys. C* **13**, 1 (2002).
7. S. Sawada, *J. Phys. A* **34**, 11253 (2001).
8. H. Lenz, C. K. Wagner and R. Sollacher, *Eur. Phys. J. B* **7**, 331 (1999).
9. R. E. Wilson, P. Berg, S. Hooper and G. Lunt, *Eur. Phys. J. B* **39**, 397 (2004).
10. K. Haesbe, A. Nahwmaa and Y. Sugiyama, *Phys. Rev. E* **69**, 017103 (2004).
11. K. Haesbe, A. Nahwmaa and Y. Sugiyama, *Phys. Rev. E* **68**, 026102 (2003).
12. H. X. Ge, R. J. Cheng and Z. P. Li, *Phys. A* **387**, 5239 (2008).
13. Y. F. Jin, M. Xu and Z. Y. Gao, *J. Comput. Nonlinear. Dynam.* **6**, 011018 (2011).
14. T. Wang, Z. Y. Gao and X. M. Zhao, *Acta Phys. Sin.* **55**, 634 (2006).
15. L. Yu, Z. K. Shi and B. C. Zhou, *Commun. Nonlinear Sci. Numer. Simulat.* **13**, 2167 (2008).
16. D. F. Xie, Z. Y. Gao and X. M. Zhao, *Commun. Comput. Phys.* **3**, 899 (2008).
17. Y. L. Mo, H. D. He, Y. Xue, W. Shi and W. Z. Lu, *Chin. Phys. B* **17**, 4446 (2008).
18. G. H. Peng and D. H. Sun, *Phys. Lett. A* **374**, 1694 (2010).
19. S. Wei, N. G. Chen and Y. Xue, *Commun. Theor. Phys.* **48**, 1088 (2007).
20. R. E. Chandler, R. Herman and E. W. Montroll, *Oper. Res.* **7**, 165 (1958).
21. M. Bando, K. Hasebe, K. Nakanishi and A. Nakayama, *Phys. Rev. E* **58**, 5429 (1998).
22. M. Treiber, A. Kesting and D. Helbing, *Phys. Rev. E* **62**, 1805 (2000).
23. M. Treiber, A. Kesting and D. Helbing, *Phys. A* **360**, 71 (2006).
24. L. C. Davis, *Phys. A* **319**, 557 (2003).
25. L. C. Davis, *Phys. Rev. E* **66**, 038101 (2002).
26. G. Orosz, R. E. Wilson and B. Krauskopf, *Phys. Rev. E* **70**, 026207 (2004).
27. G. Orosz, B. Krauskopf and R. E. Wilson, *Phys. D* **211**, 277 (2005).

28. L. Yu, T. Li and Z. K. Shi, *Phys. A* **389**, 2607 (2010).
29. H. B. Zhu and S. Q. Dai, *Phys. A* **387**, 3290 (2008).
30. H. X. Ge, X. P. Meng, R. J. Cheng and S. M. Lo, *Phys. A* **390**, 3348 (2011).
31. H. X. Ge, S. Q. Dai, L. Y. Dong and Y. Xue, *Phys. Rev. E* **70**, 066134 (2004).
32. M. C. Crossand and P. C. Hohenberg, *Rev. Mod. Phys.* **65**, 851 (1993).
33. T. Nagatani, *Phys. Rev. E* **58**, 4271 (1998).
34. T. Nagatani, *Phys. Rev. E* **59**, 4857 (1999).